ELSEVIER

Polymer 42 (2001) 1601–1612

polymer

www.elsevier.nl/locate/polymer

Structural changes during deformation of Kevlar fibers via on-line synchrotron SAXS/WAXD techniques

S. Ran[a], D. Fang[a], X. Zong[a], B.S. Hsiao[a], B. Chu[a,*], P.M. Cunniff[b]

[a]*Department of Chemistry, State University of New York at Stony Brook, Stony Brook, New York, NY 11794-3400, USA*
[b]*Department of the Army, Natick Research, Development and Engineering Center, Natick, MA 01760-5019, USA*

Received 11 February 2000; received in revised form 16 June 2000; accepted 19 June 2000

Abstract

On-line studies of structure and morphology changes in Kevlar 49 fibers during stretching were carried out using synchrotron simultaneous small-angle X-ray scattering (SAXS) and wide-angle X-ray diffraction (WAXD) techniques. A unique two-dimensional (2D) image analysis method was used to extract quantitative information of crystal, amorphous and mesomorphic fractions from 2D WAXD patterns. Results showed that about 20% of the fraction (mass) in the Kevlar 49 fiber was mesophase, 50% was crystalline and 30% was amorphous. There were transitions between crystal, amorphous and mesomorphic fractions during deformation. The crystal orientation was obtained in terms of the Herman's orientation function f_2 from the azimuthal scan of the (200) crystal reflection. The crystal orientation was found to be quite high in the Kevlar 49 fiber and increased with the stretch ratio. The fibril length and misorientation were also obtained from 2D SAXS patterns by using the Ruland method. Results showed that the fibril length decreased with the stretch ratio until 2.0% and then increased. The misorientation decreased with increasing stretch ratio.

Keywords: Kevlar 49 fiber; Poly(*p*-phenylene terephthalamide); Mesophase

1. Introduction

Kevlar aramid fiber, having a chemical structure of poly(*p*-phenylene terephthalamide) (PPD-T), is a high-performance fiber that possesses high tensile modulus, strength and thermal stability [1]. In the past two decades, its structure, morphology and the relationship between structure and properties have been studied extensively. For example, Northolt and van Aartsen [2,3] assumed that it had a centered monoclinic (pseudo-orthorhombic) unit cell and proposed a crystal lattice model of PPD-T. Haraguchi, Kajiyama and Takayanagi observed a second crystal form of PPD-T when it coagulated from a nonaqueous liquid [4]. Hindeleh et al. [5,6] and Panar et al. [7] studied the apparent crystallite size, orientation and also calculated the crystallinity from the equatorial X-ray diffraction using a conventional X-ray source; while Herglotz [8] observed the discrete scattering maximum in small-angle X-ray scattering of PPD-T. Panar et al. [7] proposed a crystalline structure model, where the stacks of crystalline layers are perpendicular to the fiber axis and separated by defect layers that are composed of chain bends and possibly half the chain ends. Pruneda et al. [9] proposed a somewhat similar defect model for the Kevlar (PPD-T) fiber. They assumed that the polymer chain ends congregate in a defect plane where breaks are more likely to occur. Panar et al. [7] proposed that the Kevlar fiber had a paracrystalline structure with the crystalline correlation length of 80–100 nm according to the results by Hindeleh et al. [5] and Barton [10]. The Kevlar fiber was observed to exhibit a pleat structure by optical microscopy with a spacing of 500–600 nm [7,11–14].

The structural changes of the aramid fibers during deformation have also been investigated in several studies by a variety of methods including mechanical testing [15–18], WAXD [19,20] and Raman spectroscopy [21–23]. Recently simultaneous WAXD/SAXS methods have become a unique tool to investigate the structure and morphology of polymer [24]. Synchrotron radiation provided us a more powerful means to carry out on-line research using simultaneous WAXD/SAXS for the study of fiber deformation [25–27]. In the present work, our goal is to obtain a more in-depth understanding of the structural changes during fiber deformation.

Recent experimental findings in polymer fibers [28–30] indicate that the fiber structure should include an intermediate phase between crystalline and amorphous fractions,

* Corresponding author. Tel.: +1-631-632-7928; fax: +1-631-632-6518.
E-mail address: bchu@notes.cc.sunysb.edu (B. Chu).

0032-3861/01/$ - see front matter
PII: S0032-3861(00)00460-2

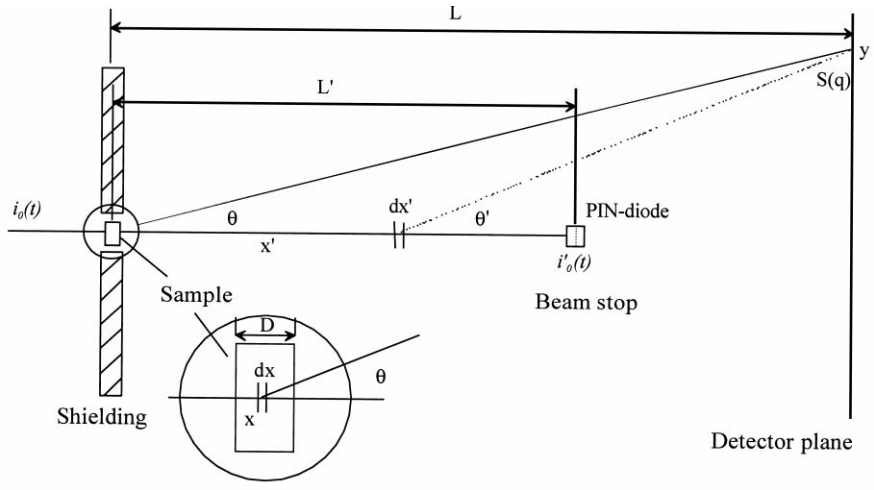

Fig. 1. Schematic diagram of X-ray detection setup using a PIN-diode beam stop to correct the air scattering. In this figure, *x*-axis represents the direction of the incident beam. θ is the scattering angle. *yz* denotes the detection plane, perpendicular to the *x*-axis. L' is the distance between center of the sample holder and the beam stop; L is the distance between center of the sample holder and the detection plane; $i_0(t)$ is the incident X-ray intensity at time t before the sample; $i'_0(t)$ is the transmitted X-ray intensity at time t after the sample and air path L'; D is the sample thickness. x is the integration variable for the sample; x' is the integration variable for the air path between the sample and the beam stop.

which may be due to the lattice dislocations or one- and two-dimensional (1D and 2D) disordering of polymer chains in the drawn fibers. The intermediate phase (mesophase) represents a state of order between the zero long-range ordering (amorphous state) and the three-dimensional (3D) crystalline ordering. The mesophase has been reported in some polymer fibers, such as polypropylene [31–33], polyethylene [28] and PET [30]. Although the mesophase in the Kevlar fibers has not been discussed extensively, Dobb et al. [34] have stated that there was evidence for 2D ordering in the Kevlar fibers based on the layer-like streaking in electron diffraction patterns. English et al. [35–39] studied the structural dynamics of the Kevlar fiber using ^{2}H NMR spectroscopy and pointed out that the dynamics was quite heterogeneous in structure. Thus, a less perfectly ordered structure could exist, probably from chains residing mostly at or close to the surface of the crystallites. The difficulty for the study of the mesophase is that no straightforward method that is able to extract the fraction of the mesophase quantitatively exists. In this study, we introduce an integrative X-ray fiber diffraction image analysis approach that based on the model is capable of extracting the fraction of the mesophase quantitatively. We will also illustrate other additional methods that can extract structural and morphological information from the 2D WAXD/SAXS patterns.

2. Experimental

The fibers studied were commercial Kevlar 49 fiber. Synchrotron measurements were carried out at the State University of New York (SUNY) X3A2 beam line in the National Synchrotron Light Source (NSLS), Brookhaven National Laboratory (BNL). The wavelength used was 1.54 Å. A 3-pinhole collimator system [40,41] was used to reduce the beam size to 0.6 mm in diameter. The 2D WAXD patterns were recorded by a MAR CCD X-ray detector (MARUSA) for quantitative image analysis. Separate simultaneous SAXS and WAXD patterns were recorded using Fuji™ HR-V imaging plates (200×250 mm^2), which were then individually and separately digitized by using a Fuji™ BAS 2000 IP imaging plate scanner [24]. The WAXD imaging plate images were used to compare with the CCD images, but were not analyzed. Only the SAXS images were studied in this work. The sample to detector distance for WAXD was 90.7 mm, which was calibrated using an Al_2O_3 standard. The sample to detector distance for SAXS was 1156 mm. The collection time for both WAXD and SAXS measurements was 2 min. In order to make an accurate correction of air scattering, a PIN-diode beam stop was used. The PIN-diode used was a silicon based photon diode with a diameter of 3.0 mm. The sensor portion contained a 1.5×1.5 mm^2 rectangle silicon chip. The PIN-diode recorded the transmitted intensity after the fiber, which was used to estimate the effect of sample absorption (see Section 3.1 for details).

The stretching unit was a modified tabletop stretching apparatus from Instron Inc. (model 4410). The modification allowed the sample to be symmetrically stretched. The symmetric stretching mode assured that the focused X-rays always illuminated the same position on the fiber during deformation. The chosen stretching speed was 3 mm/min in this study. After having reached the desired stretch ratio, the fiber was held for 2 min for image collection and was then subjected to the next stretch ratio. For SAXS measurement, the fiber was held for an additional 5 min allowing the image to be digitized by the scanner.

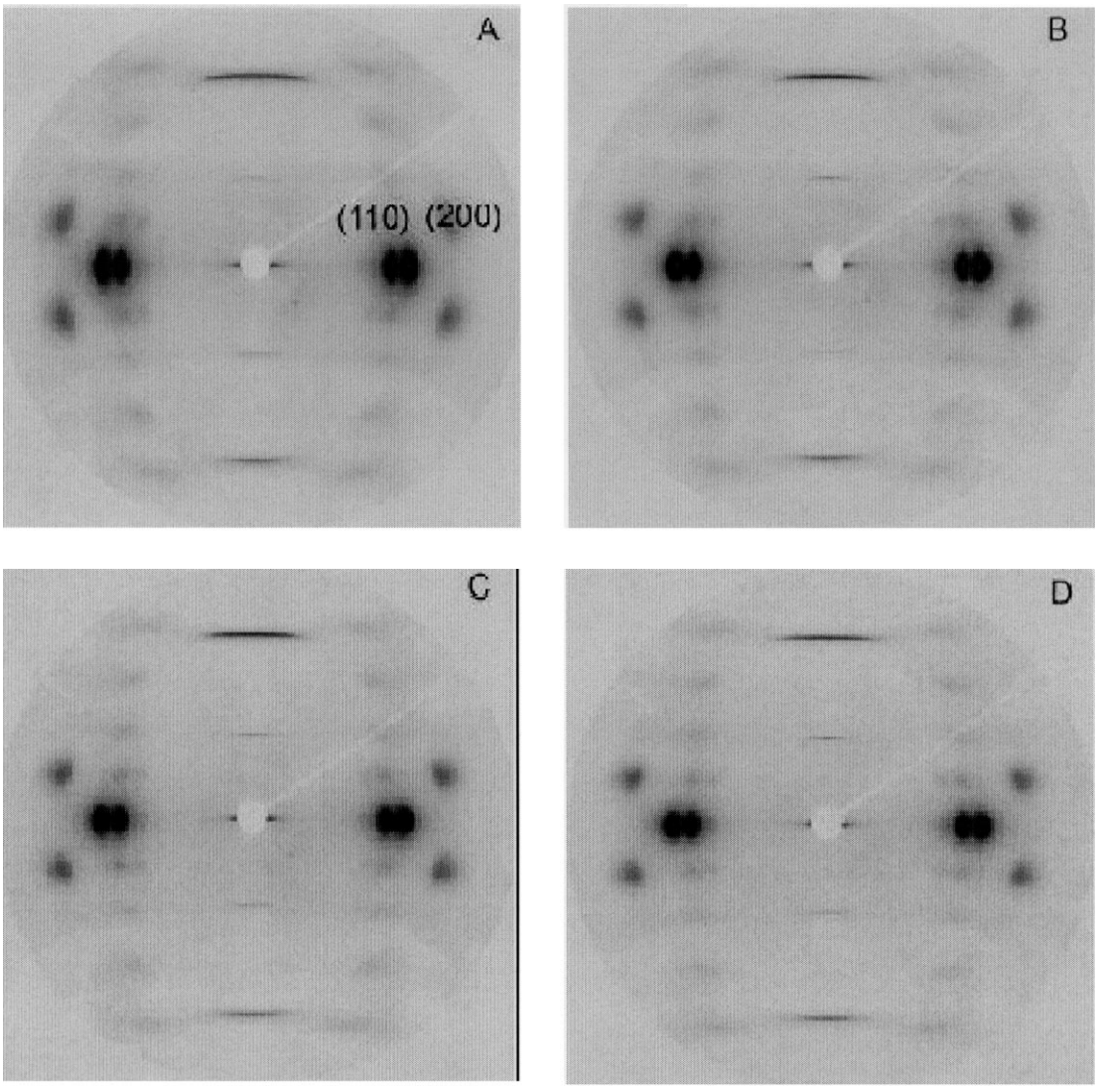

Fig. 2. 2D WAXD patterns of Kevlar 49 fibers at four different stretch ratios: (A) 0%; (B) 0.9%; (C) 2.07%; (D) 3.00%.

3. Data analysis

3.1. Background correction

In the data analysis of 2D WAXD and SAXS patterns, the elimination of background scattering from the air pathway and instrumentation is critical and non-trivial. In addition, the air scattering also changes due to the sample thickness change and incident beam fluctuation during deformation. In this study we have developed a new method to solve this problem using the PIN-diode beam-stop with the following procedures.

As shown in Fig. 1, we assume that the incident X-ray beam $i_0(t)$ is stable in shape, but fluctuates in time. With the PIN-diode in the beam-stop position, the measurement and background correction can be accomplished by using the following two steps.

Step 1. Measurement without sample (background scattering)

As the PIN-diode is placed at a distance L' from the center of the sample holder, the image registration plane is located at L, the integrated beam intensity (I_0') measured by the PIN-diode over time T_1 is

$$I_0' = \eta_p \int_0^{T_1} i_0(t)\, e^{-\mu_0 L'}\, dt = e^{-\mu_0 L'} \eta_p II_{01} \quad (1)$$

$$II_{01} = \int_0^{T_1} i_0(t)\, dt \quad (2)$$

where μ_0 is the absorption coefficient of X-ray by air and we assume μ_0 is not a function of time t, η_p is the quantum detection coefficient of the PIN-diode and II_{01} is the beam intensity integration (IC_0) *before* the air absorption.

Let us examine a point at y on the scattering registration

plane (2D detector plane). The scattering is mostly contributed from air that the X-ray passes after the sample holder (without sample). The measured scattered intensity ($I_s^a(y)$, with superscript 'a' denoting air scattering) can be expressed as

$$I_s^a = \eta_d \int_0^{L'} \int_0^{T_1} i_0(t)\, e^{-\mu_0 x'}\, dt S_a(q')\, e^{-\mu_0((L-x')/\cos\theta')}\, dx'$$
$$= \eta_d I I_{01} \bar{S}_a(\bar{q}) \quad (3)$$

where η_d is the quantum coefficient of the detector. The term $\bar{S}_a(\bar{q})[\equiv \int_0^{L'} \exp(-\mu_0(x'+(L-x')/\cos\theta')))S_a(q')\, dx']$ can be considered as an averaged scattering term from an averaged $\bar{q}$ value due to air scattering. The ratio of the two measured quantities (I_s^a (from the detector), I_0' (from the PIN-diode)) without the sample is Eq. (3)/Eq. (1) and becomes:

$$I_s^a/I_0' = \frac{\eta_d}{\eta_p}\, e^{\mu_0 L'} \bar{S}_a(\bar{q}). \quad (4)$$

Step 2. Measurement with sample and air

When the sample is in view, the X-ray beam is further absorbed by the sample. If the sample is not too thick, we can assume that the air path has remained essentially the same as the case without the sample. To simplify the calculation, we assume that the sample is a flat film with a thickness D. The measured intensity by the PIN-diode over a period T_2 becomes

$$I_0 = \eta_p \int_0^{T_2} i_0(t)\, e^{-\mu_0 L'}\, e^{-\mu_s D}\, dt = e^{-(\mu_0 L' + \mu_s D)} \eta_p I I_{02} \quad (5)$$

with $II_{02} = \int_0^{T_2} i_0(t)\, dt$.

The intensity measured at point y due to air and sample scattering, as denoted by the superscript a + s, on the 2D detector plane now becomes

$$I_s^{a+s} = \eta_d \int_0^D dx \int_0^{T_2} i_0(t)\, e^{-\mu_s x}\, dt S_s(q)$$
$$\times e^{-\mu_s((D-x)/\cos\theta))}\, e^{-\mu_0(L/\cos\theta)} + \eta_d e^{-\mu_s D} I I_{02} \bar{S}_a(\bar{q})$$
$$= \eta_d I I_{02}\, e^{-\mu_0(L/\cos\theta)} F(D, \cos\theta) S_s(q)$$
$$+ \eta_d\, e^{-\mu_s D} I I_{02} \bar{S}_a(\bar{q}) \quad (6)$$

where $F(D, \cos\theta) = \int_0^D \exp(-\mu_s(x + (D-x)/\cos\theta))\, dx)$ and we have assumed $D \ll L$. Now the ratio of I_s^{a+s} to I_0 is

$$I_s^{a+s}/I_0 = \frac{\eta_d \exp(-\mu_0(L/\cos\theta)) F(D, \cos\theta)}{\eta_p \exp(-\mu_0 L' - \mu_s D)} S_s(q) + (I_s^a/I_0') \quad (7)$$

The quantity $S_s(q)$ is the "corrected" scattering function from the sample. It can be explicitly expressed as

$$S_s(q) = \frac{\eta_p \exp(-\mu_0(L' - (L/\cos\theta)) - \mu_s D)}{\eta_d F(D, \cos\theta)} \left(\frac{I_s^{a+s}}{I_0} - \frac{I_s^a}{I_0'} \right) \quad (8)$$

Thus, by measuring the four parameters (I_0', I_s^a, I_0, and I_s^{a+s}) using the same setting and with $F(D, \cos\theta)$ one can obtain the scattering function $S_s(q)$ with the proper background correction.

From Eq. (8), it is clear that the measured intensity has to be corrected not only by air background scattering subtraction but also by the sample thickness and the cos θ values. In this work, the thickness of the Kevlar 49 fiber is quite small and the thickness change is also small due to the small stretch ratio. Thus the effect of sample thickness (D) can be neglected. Furthermore, we find the effect of cos θ is also small.

Fig. 2 illustrates the 2D WAXD patterns of the Kevlar fiber obtained at different draw stretch at room temperature. These patterns have been corrected for the incident beam fluctuation and air scattering using the above procedure. From these patterns, the information of the crystal orientation and the fractions of crystal, amorphous and mesomorphic phases can be obtained through the following data analysis schemes.

3.2. Crystal orientation

If we only consider the crystal phase, its orientation can be defined as the relationship of some crystallographic direction to an external reference frame. The drawing direction (along the fiber axis) is often defined as the reference direction. In the Kevlar fiber, the (200) plane is often used for the calculation of crystal orientation [1,26]. For a set of *hkl* planes, the orientation, expressed as $\langle \cos^2 \phi \rangle_{hkl}$, can be calculated mathematically using the following equation [42]:

$$\langle \cos^2 \phi \rangle_{hkl} = \frac{\int_0^{\pi/2} I(\phi) \cos^2 \phi \sin \phi\, d\phi}{\int_0^{\pi/2} I(\phi) \sin \phi\, d\phi} \quad (9)$$

where ϕ is the azimuthal angle and $I(\phi)$ is the scattered intensity along the angle ϕ. The orientation parameter $\langle \cos^2 \phi \rangle_{hkl}$ has the value of unity when the normal of the reflection plane *hkl* is oriented parallel to the reference direction, and a value zero when the normal of this plane is perpendicular to the reference direction. Very often the parameter f_2, the so-called Herman's orientation function, is used to describe the degree of orientation.

$$f_2 = \frac{3\langle \cos^2 \phi \rangle - 1}{2} \quad (10)$$

where f_2 has the value of unity when the normal of the reflection plane is parallel to the reference direction, and a value -0.5 when the normal is perpendicular to the reference direction, and a value zero when there is random orientation in the sample.

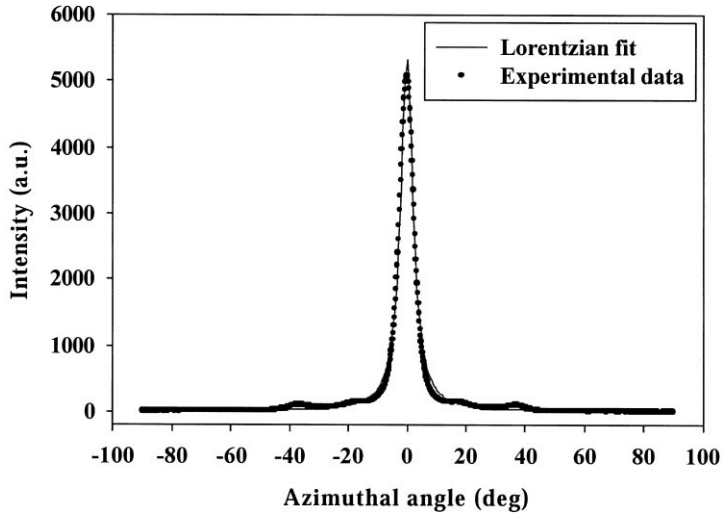

Fig. 3. A representative azimuthal intensity $I(\phi)$ profile of the (200) reflection and its Lorentzian fit overlaid with the azimuthal intensity data obtained from the stretched fibers with a stretch ratio of 3.0%. The dots represent the experimental data and the solid line corresponds to the Lorentzian fit

$$I(\phi) = 4.4 + \frac{5315.3}{1 + ((\phi + 0.06)/2.6)^2}.$$

3.3. Fractions of crystal, mesomorphic and amorphous phases

For drawn fibers, the 2D WAXD pattern corrected for the background and the air scattering can be deconvoluted into two fractions: isotropic and anisotropic parts. The isotropic part includes the scattering from the amorphous phase and the Compton scattering from chemical structure which is usually small at typical detection angular range and may be ignored. The isotropic fraction $A_{iso}(s)$ can be obtained using the following method. Starting from the center of the scattering pattern, a series of azimuthal scans can be obtained as a function of s ($s = 2\sin(\theta/2)/\lambda$ is the scattering vector and θ is the scattering angle). The minimum intensity is determined from each azimuthal scan at a value of s. All of the minimum intensities at different values of s thus represent the envelope of the isotropic contribution.

The deconvolution of the anisotropic fraction $A_{an}(s,\phi)$ then can be calculated from the following equation:

$$A_{an}(s, \phi) = A - A_{iso}(s) \tag{11}$$

where A is the total scattering. Note that $A_{iso}(s)$ is not a function of ϕ, but $A_{an}(s,\phi)$ is.

The anisotropic fraction can be further deconvoluted into mesomorphic and crystal fractions by using a 2D peak fit method. Assuming each peak in both the crystal phase or the mesophase can be described by a 2D function such as Gaussian, Lorentzian, Pearson VII or Pseudo-Voigt, the generalized expression for each 2D function becomes [43]

$$\text{Gaussian}: \quad f = h \exp\left(-\left(\frac{x_0 - x}{\omega_x}\right)^2 - \left(\frac{y_0 - y}{\omega_y}\right)^2\right) \tag{12}$$

$$\text{Lorentzian}: \quad f = \frac{h}{\left(1 + \left(\frac{x_0 - x}{\omega_x}\right)^2 + \left(\frac{y_0 - y}{\omega_y}\right)^2\right)} \tag{13}$$

$$\text{Pearson VII}: \quad f = \frac{h}{\left(1 + \frac{(x_0 - x)^2}{\omega_x^2 n} + \frac{(y_0 - y)^2}{\omega_y^2 n}\right)^n} \tag{14}$$

$$\text{Pseudo-Voigt}: \quad f = g(Gaussian) + (1 - g)(Lorentzian) \tag{15}$$

where the subscript "0" represents the peak position, ω is the full width at half maxima, h represents the height of the peak, n is the constant which is between 6 and 25 and g is the Gaussian fraction of the pattern. In the polar coordinate system, the following relations exist: $x = r\sin\phi$ and $y = r\cos\phi$. The widths along the r axis and ϕ axis are related to the size and orientation information of each reflection, respectively.

4. Results and discussion

The WAXD patterns from fiber deformed at different stretch ratios are shown in Fig. 2. Two strong reflections located on the equator can be indexed as (110) and (200), respectively. These two reflections show a small spread along the azimuthal direction indicating that the fiber has a high degree of crystal orientation along the fiber axis. The spread became narrower with increasing stretch ratio indicating that the orientation increases with increasing stretch ratio. The successive layer lines associated with the molecular repeat spacing of the Kevlar molecules stacked in the

Table 1
Results of the calculation of the orientation factors

Draw ratio (%)	r^{2a}	$\langle\cos^2\phi\rangle_{200}$	f_2
0	0.997	0.87	0.80
0.9	0.997	0.89	0.83
2.1	0.997	0.92	0.87
3.0	0.997	0.93	0.90
4.0	0.998	0.82	0.72

[a] r^2 (coefficient of determination) is the measure of closeness of a regression to the data, where $r^2 = 1$ is a perfect fit. Specifically, it is the covariance divided by the product of the sample standard deviations.

meridional direction became straightened by stretching. This observation is consistent with an increase in the crystal orientation. In this study, we used the equatorial (200) reflection to monitor the total crystal orientation changes, using the method of azimuthal profile of intensity as outlined previously [44,45].

A representative azimuthal intensity profile of reflection (200) obtained from the stretched fibers at a draw ratio of 3.0% is shown in Fig. 3. It is seen that there are two small additional peaks at each side of the reflection (200) at azimuthal angles about ± 17 and $\pm 37°$. These small peaks are due to the other off equatorial axis reflections when the azimuthal scan is taken. These small peaks can be fitted with some functions and be eliminated from the main (200) peak. The intensity profile $I(\phi)$ of the reflection (200) is fitted with a Lorentzian function (Fig. 3), which yields a good fit with the r^2 coefficient of about 0.997.

$$I(\phi) = y_0 + \frac{a}{1 + ((\phi - \phi_0)/b)^2} \tag{16}$$

In this equation, y_0, ϕ_0, a, b are fitting parameters and b is the full width at half maximum of the peak.

The orientation factor, $\langle\cos^2\phi\rangle_{200}$ and f_2, calculated from the fitted profile, are summarized in Table 1 and plotted in Fig. 4. The original non-stretched fiber showed a high degree of crystal orientation ($f_2 = 0.8$), which could be responsible for the high modulus in the fiber. The orientation was found to increase with increasing stretch ratio. However, as the stretch ratio reached 4.0% the orientation was seen to decrease dramatically. It is known that the Kevlar 49 fiber has a typical draw-to-break ratio of about 3.0% [1]. A stretch ratio of 4.0% is probably fairly close to the breaking point. Thus, it is logical to conclude that, at 4.0% stretching, some of the chains were broken, resulting in a decrease in the total crystal orientation. The Kevlar fiber is suggested to exhibit a skin-core differential in density, voidage and fibrillar orientation resulting from the fiber coagulation process [46–48]. The orientation in our calculation is an average value for the sample after subtraction of the amorphous contribution.

At this point, we should mention that the typical numerical integration method to calculate $\langle\cos^2\phi\rangle_{200}$ or f_2 is not sensitive to the small changes in the azimuthal half width. Fluctuations associated with the noise in the intensity profile can lead to a relative large error in the numerical integration calculation.

In this study a novel image analysis method has been introduced to deconvolute the fractions of crystal, mesophase and amorphous phases. As discussed earlier, the 2D WAXD pattern after correction of air scattering and beam fluctuation can be deconvoluted to an isotropic part and an anisotropic part. A 2D peak fit procedure is then used to separate the crystal phase and the mesophase from the anisotropic fraction of the scattering. Considering that the mesophase has only one or 2D ordering packing along the stretching direction, the mesophase can only contribute to the scattered intensities along the equatorial direction. In the 2D deconvolution procedure, we first select a region that contains the main reflections (110 and 200) and the oriented

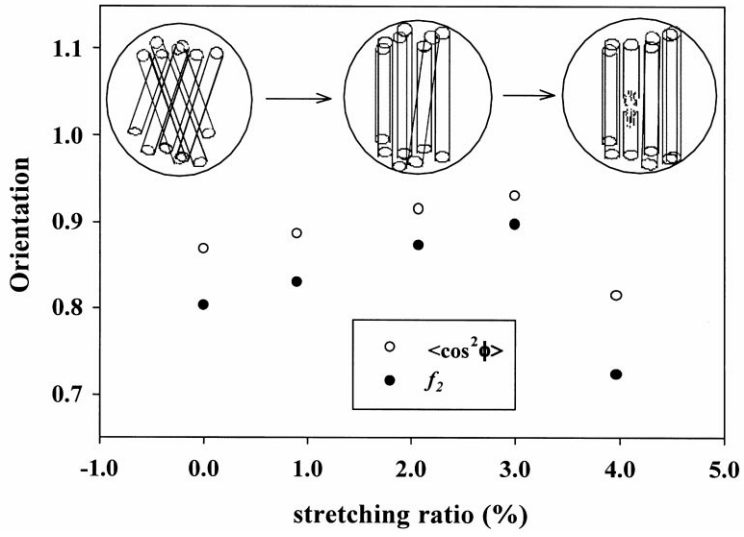

Fig. 4. Variation of the orientation factor and the Herman orientation function f_2 as a function of stretch ratio.

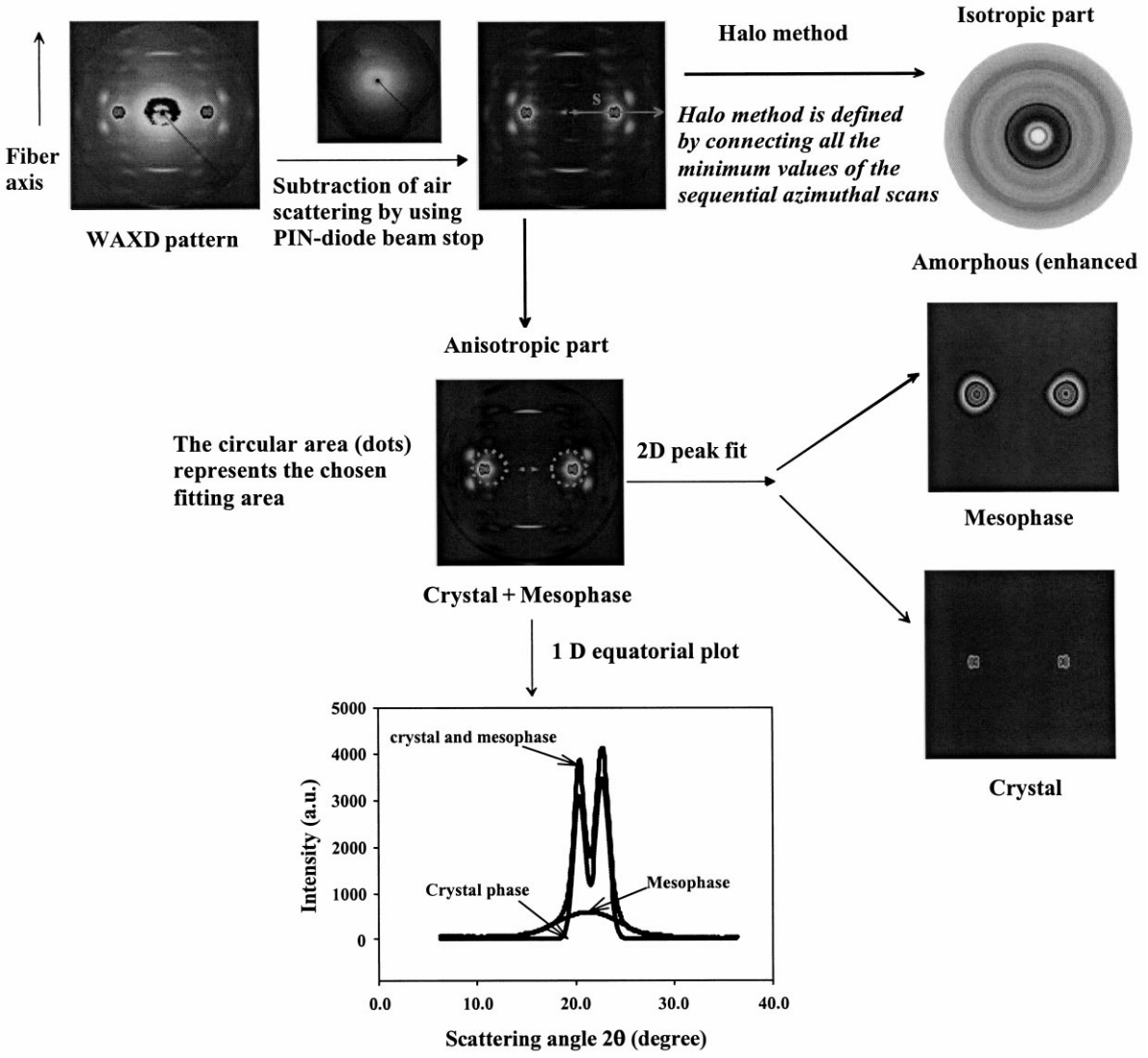

Fig. 5. Procedures for deconvolution of the crystal phase, mesophase and amorphous phase from 2D WAXD patterns.

diffused scattering background along the equator. Assuming that both the crystal phase and the mesophase can be described as 2D Gaussian functions (Eq. (12)) or other functions, then the two crystal reflections ((110) and (200)) and the mesophase background can be separated numerically. The typical mesophase calculated in such a fashion is more disordered, as the crystal phase has a regular lateral registration forming sharper peaks. The areas of the crystal and the mesophase reflections calculated can be used to estimate the fractions of the two different phases. The error level of the 2D peak fit function is less than 2%. Fig. 5 shows the original 2D WAXD pattern and the respective procedures of actual handling of the data. The 2D patterns and 1D plots of the crystal and the mesophase after 2D peak fit are also shown in Fig. 5.

Fig. 6 shows the changes in the crystal, mesomorphic and amorphous phases during deformation as a function of stretch ratio. It is seen that more than 20% of the fraction (mass) in the fiber can be considered as the mesophase implying that 20% of the chains are in the intermediate state between the crystalline and the amorphous phases. However we do not know exactly the location of the mesophase in the fiber. In view of the reported morphology and the crystallinity in the Kevlar fiber thus far [34–39], we speculated that the mesophase could represent the highly oriented fraction of the chains with lattice registrations too low to be considered as crystalline. The loss of the 3D regularity may occur when occasional defects in the crystal packing are incurred. An amorphous fraction of near 30% may represent the boundary fraction of the chains between the crystal fibrils (or the crystals) and the mesophase. This fraction corresponds to the defect layer proposed by Panar et al. and Pruneda et al. [7,9]. English et al. pointed out that a large fraction (~40%) of the chains in the Kevlar fibers resided on the surface of the crystals since the crystal size was quite small. Some of these chains (unoriented) on the

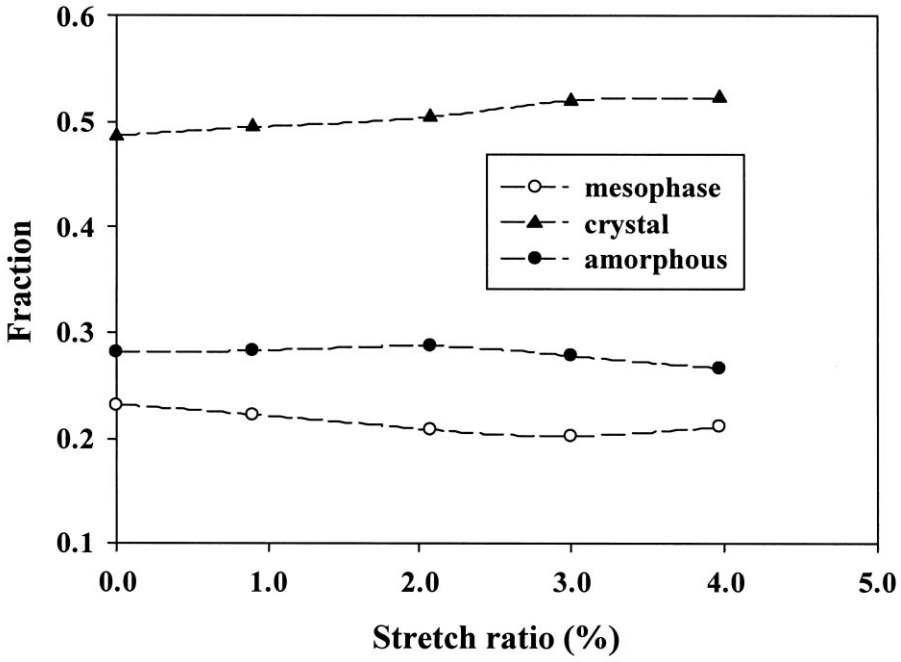

Fig. 6. Variation of fractions of crystal, amorphous and mesomorphic phases as a function of stretch ratio.

crystal surface may result in an amorphous structure, with the fraction value being quite similar to our estimation (30%).

The fraction of the mesophase is less than the fraction of the amorphous phase. The chains in the mesophase have only one or 2D ordering and pack along the fiber axis. Such a molecular arrangement in the mesophase may result in higher tenacity and higher elongation than the crystal fraction. However, since the total mass fraction of the mesophase is low (20%), the effect of the mesophase on the final mechanical properties may be limited. For future development of high strength fibers with higher tenacity, it is probably desirable to increase the fraction of the mesophase. It is noted that the variations of the mass fraction in the amorphous phase, crystal phase and mesophase are relatively small because the deformation employs small stretch ratios and takes place in room temperature. However, there is evidence indicating that the conversion among crystal, amorphous and mesomorphic fractions could occur. For example, the crystallinity was found to increase with stretch ratio. The fraction for the mesophase decreased and that for the amorphous phase increased before the stretch ratio reached 3.0%. These findings indicate that some of the mesophase may be converted to the crystal phase and some others to the amorphous phase. These results suggest that the mesophase is not a stable phase, i.e. it is metastable. Stretching obviously provides the kinetic energy that either facilitates the lateral registration forming a 3D crystal

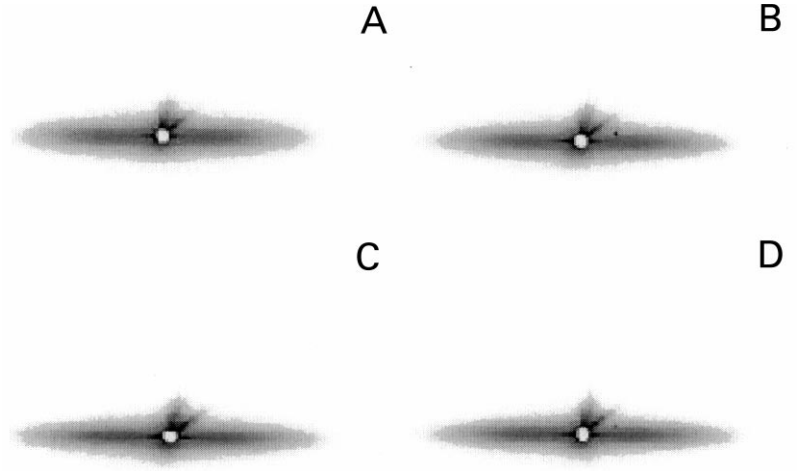

Fig. 7. 2D SAXS patterns of Kevlar 49 fibers at four different stretch ratios: (A) 0%; (B) 1.26%; (C) 2.16%; (D) 3.00%.

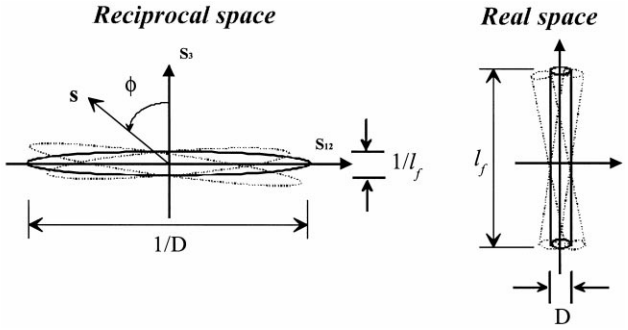

Fig. 8. Schematic diagram of crystal fibril with a length (l_f) in reciprocal space and in real space.

structure or totally destroys the ordering of the mesophase. Above the stretch ratio of 3.0% it is seen that the amount of the mesophase increases and that of the amorphous phase decreases. The chains in the amorphous phase (even in the crystal/crystal boundary) can be oriented at high draw ratios and can be packed with some kind of ordering to form the mesophase.

In the following section, we intend to illustrate the corresponding morphological changes extracted by the SAXS technique. Fig. 7 shows the 2D SAXS patterns of the Kevlar 49 fibers obtained at different draw ratios. The common feature seen in these patterns is that the SAXS intensity has a shape of a streak along the equator and there is no detectable scattering along the meridional direction. The streak pattern indicates that the superstructure of the Kevlar 49 fibers is mainly a fibrillar structure, with no trace of lamellar morphology. This result is somewhat different from the works by Panar et al. [7]. They observed that there were ordered lamellae in the superstructure of the Kevlar fibers (although the fraction could be small). The work done by Grubb et al. also did not show any lamellar structure in the Kevlar 49 and Kevlar 149 fibers [49], which is consistent with our finding. We believe the different morphology observed in the Kevlar fiber may be due to the change(s) in the manufacturing process of the fiber.

The interpretation of the equatorial scattering in SAXS is more complicated since it may contain several contributions including the microfibrillar structure, voids morphology and the surface reflection/scattering of the fiber. Grubb et al. [49] pointed out that the scattering objects in the Kevlar 49 were mainly associated with the microfibrillar structure, not from the void morphology. We are in complete agreement with them, as one of us has carried out SAXS study of the Kevlar 49 fibers soaked with solvents of different density, and the shape and the intensity of the streak patterns were always about the same. Dobb et al. [34] also concluded that the Kevlar fiber exhibited no obvious voids, which was different from carbon fibers. The streak on the equator was produced by scattering objects extended along the fiber direction. If the objects were perfectly aligned in the fiber direction and had a finite length L, then the angular width of the streak (measured in the direction of the fiber axis) should be constant and the width should not be a function of the scattering angle. However, in most cases, this is not true, implying that both the size distribution and the misorientation of the scattering object have contributed to the streak profile. We have used the following method proposed by

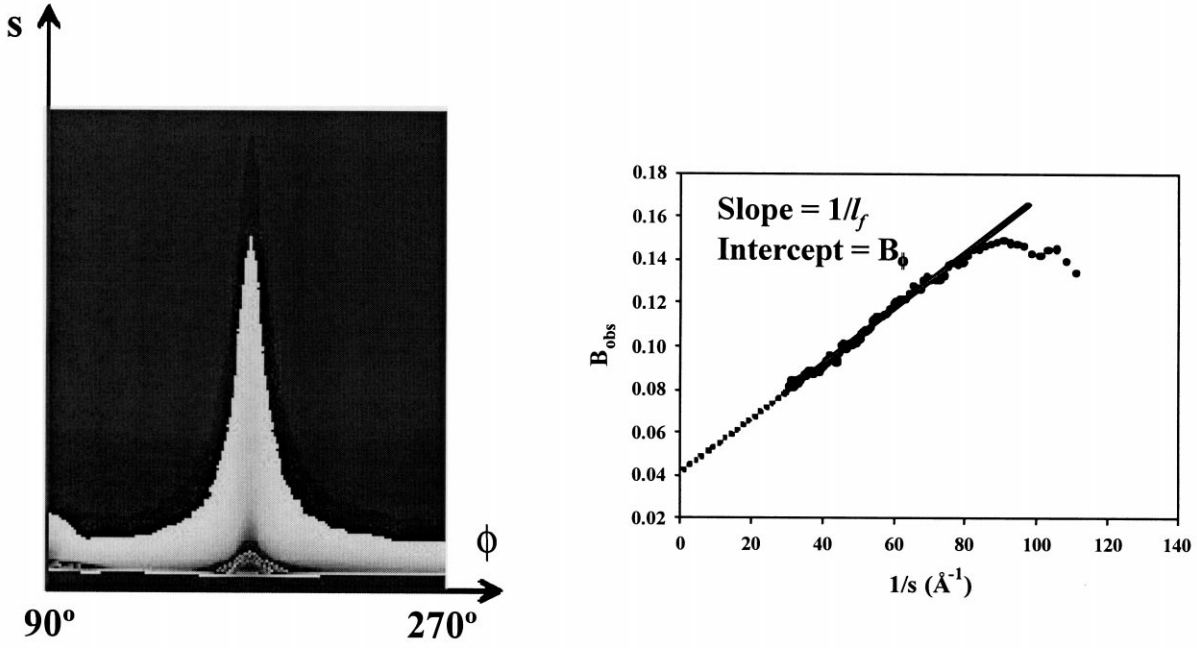

Fig. 9. Schematic presentation of azimuthal scans of the equatorial streak and the corresponding Ruland plot (B_{obs} vs s^{-1}, where B_{obs} is the full width at half maximum of the azimuthal scan).

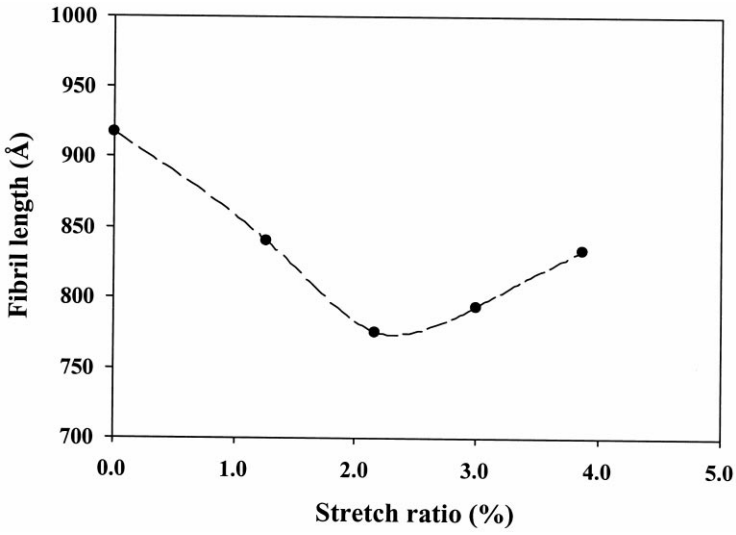

Fig. 10. Fibril length changes of the Kevlar 49 fiber at different stretch ratios.

Ruland [50] to analyze the intensity distribution in order to obtain the information of the average fibril length and the fibril misorientation from the fiber axis (shown in Fig. 8). We have determined the angular spread (B_{obs}) of each azimuthal profile as a function of s. From these angular spread (Fig. 9), the fibril length (l_f) and the misorientation width (B_ϕ) can be obtained using the following equation.

$$B_{obs} = \frac{1}{l_f s} + B_\phi \qquad \text{(Cauchy–Cauchy)} \tag{17}$$

where B_{obs} is actually the full width at half maximum of the azimuthal profile from the equatorial streak fitted with a Lorentzian function. The expression for the Gaussian function is as follows:

$$B_{obs}^2 = \left(\frac{1}{l_f s}\right)^2 + B_\phi^2 \qquad \text{(Gaussian–Gaussian)} \tag{18}$$

The Lorentzian function gave a much better fit. So we used Eq. (17) for the analysis. The fibril length (l_f) thus could be obtained from the slope of the B_{obs} vs. s^{-1} plot and the intercept (B_ϕ) yields the fibril misorientation width (Fig. 9). We took only the slope of the intermediate values of s ($0.01 < s < 0.034$), corresponding to the q values between 0.063–0.21 (Å^{-1}) for the analysis. In the larger q range, the intensity became very weak, leading to large errors.

Fig. 10 shows the fibril length of the Kevlar 49 fiber at different stretch ratios. Grubb et al. reported that the fibril length of the Kevlar 49 was about 700 Å [49] and our values are in general agreement. It was seen that the fibril length decreased before the stretch ratio reaches 2.0% and then increased. We assume that the fibril length in the fibers has a distribution and the measured value represents a mean quantity. It is conceivable that when the fiber is stretched, some long fibrils may break because they probably carry the most loading. To decrease the average value of l_f by about 20%, the total breakage can be very small. The breakage can occur if some defects are incurred in the crystal fibrils. At high strains, the increase in the average fibril length may be due to the conversion of the amorphous phase to the crystals or to the mesophase as observed earlier by WAXD.

Fig. 11 shows the width of the misorientation of the fibril at different stretch ratios. The misorientation was found to decrease with increasing stretch ratio until 3.0%, indicating an increase in the orientation of the fibrils. The misorientation was found to increase at stretch ratios above about 4.0%, which could be attributed to the breakage of some fibrils. This result is consistent with earlier results obtained from WAXD (Fig. 4).

5. Conclusions

A novel 2D image analysis method was introduced to extract quantitative information about the fractions of the crystal, amorphous and mesomorphic phases from WAXD fiber patterns. The average percentage of the mesophase in the Kevlar 49 aramid fiber using this method was about 20%, with the corresponding crystal phase being about 50% and the amorphous phase being about 30%. The mesophase may represent the highly oriented fraction of the chains with lattice registrations too poor to be considered as crystalline. It was found that the crystal, mesophase and amorphous phases can undergo conversions with increasing stretch ratio, although the typical conversion ratio was small. The average crystal orientation was obtained in terms of $\langle \cos^2 \phi \rangle$ and the Herman orientation function f_2. The crystal orientation was quite high in the original Kevlar 49 fiber but increased further with increasing stretch ratio until it broke. The fibril length and misorientation of the fibril were obtained from 2D SAXS patterns using the

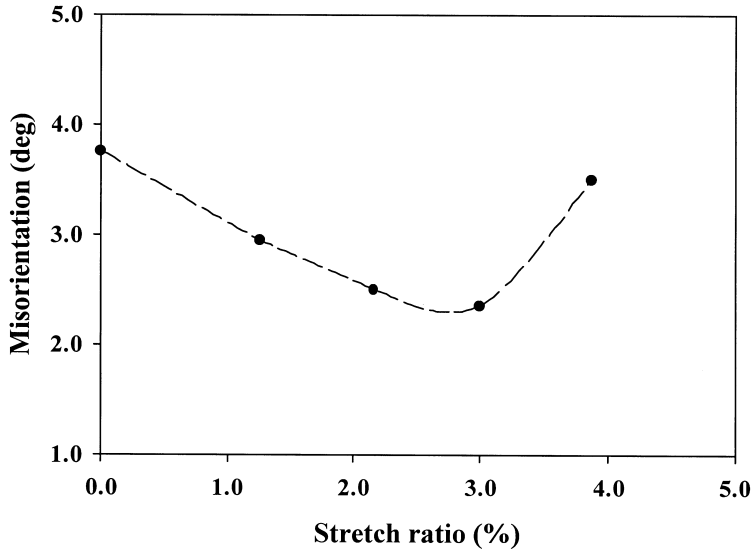

Fig. 11. Misorientation breadth of fibril at different stretch ratios.

Ruland method. The fibril length was found to decrease with increasing stretch ratio until about 2.0% and then it increased with increasing stretch ratio. The misorientation of the fibril decreased with increasing stretch ratio, indicating that the total orientation increased.

Acknowledgements

The authors are grateful for the financial support of this work by a grant from the US Army Research Office (DAAG559710022). A discussion with Dr R. Barton from DuPont was most useful for the preparation of this work.

References

[1] Yang HH. Kevlar aramid fiber. Chichester, UK: Wiley, 1993 (200pp).
[2] Northolt MG. Eur Polym J 1974;10:799.
[3] Northolt MG, van Aartsen JJ. J Polym Sci, Polym Lett Ed 1973;11:333.
[4] Haraguchi K, Kajiyama T, Takayanagi M. J Appl Polym Sci 1979;23:903.
[5] Hindeleh AM, Halin NA, Zig KA. J Macromol Sci, Phys B 1984;23(3):289.
[6] Hindeleh AM, Abdo ShM. Polymer 1989;30:218.
[7] Panar M, Avakian P, Blume RC, Gardner KH, Gierke TD, Yang HH. J Polym Sci, Polym Phys Ed 1983;21:1955.
[8] Herglotz HK. J Colloid Interface Sci 1980;75:105.
[9] Pruneda CO, Steele WJ, Kershaw RP, Morgan RJ. Polym Prepr ACS Div Polym Chem 1981;22:216.
[10] Barton R. J Macromol Sci, Phys B 1985;24:119 (ACS National Meeting Philadelphia, PA, 1984).
[11] Hagege R, Jarrin M, Sutton M. J Microsc 1979;115:65.
[12] Dobb MG, Johnson DJ, Saville BP. J Polym Sci, Polym Phys Ed 1977;15:2201.
[13] Dobb MG. In: Watt W, Perov BV, editors. Handbook of composites, Strong fibers, vol. 1. Amsterdam: Elsevier, 1985 (chap. XVII).
[14] Li LS, Allard LF, Bigelow WC. J Macromol Sci, Phys B 1983;22(2):269.
[15] Northolt MG, Hout Rvd. Polymer 1985;26:310.
[16] Northolt MG. Polymer 1980;21:1199.
[17] Allen SR, Roche EJ. Polymer 1989;30:996.
[18] Young RJ, Lu D, Day RJ, Knoff WF, Davis HA. J Mater Sci 1992;27:5431.
[19] Li Y, Wu C, Chu B. J Polym Sci, Part B: Polym Phys 1991;29:1309.
[20] Chu B, Wu C, Li Y, Harbison GS, Roche EJ, Allen SR, Mcnulty Philips JC. J Polym Sci, Part C: Polym Lett 1990;28:227.
[21] Prasad K, Grubb DT. J Appl Polym Sci 1990;41:2189.
[22] Chang C, Hsu SL. Macromolecules 1990;23:1484.
[23] Penn L, Milanovich F. Polymer 1979;20:31.
[24] Hsiao BS, Chu B, Harney P, Kennedy AD, Leach RA. J Appl Crystallogr 1997;30:1084.
[25] Dobb MG, Johnson DJ, Saville BP. J Polym Sci, Polym Phys Ed 1977;15:2201.
[26] Alexander LE. X-ray diffraction methods in polymer science. New York: Wiley, 1969 (582 pp).
[27] Bruckner S, Meille SV, Petraccone V, Pirozzi B. Prog Polym Sci 1991;16:361.
[28] Androsch R, Blackwell J, Chvalun SN, Wunderlich B. Macromolecules 1999;32(11):3735.
[29] Androsch R, Wunderlich B. 26th Proc. Conf. North Am. Therm. Anal. Soc., 1998. p. 469.
[30] Wunderlich B. Macromol Symp 1997;113:51.
[31] Bruckner S, Meille SV, Petraccone V, Pirozzi B. Prog Polym Sci 1991;16:361.
[32] Corradini P, DeRosa C, Guerra G, Petraccone V. Polym Commun 1989;30:281.
[33] Phillips RA, Wolkowicz MD. In: Edward Jr. PM, editor. Polypropylene handbook, Munich: Hanser, 1996 (419 pp).
[34] Dobb MG, Johnson DJ, Saville BP. J Polym Sci, Polym Symp 1977;58:237.
[35] Schaefer DJ, Schadt RJ, Gardner KH, Gabara V, Allen SR, English AD. Macromolecules 1995;28:1152.
[36] Schadt RJ, Cain EJ, Gardner KH, Gabara V, Allen SR, English AD. Macromolecules 1993;26:6503.
[37] Schadt RJ, Gardner KH, Gabara V, Allen SR, Chase DB, English AD. Macromolecules 1993;26:6509.
[38] Jackson CL, Schadt RJ, Gardner KH, Chase Allen SR, Gabara V, English AD. Polymer 1994;35(6):1123.
[39] Cain EJ, Gardner KH, Gabara V, Allen SR, English AD. Macromolecules 1991;24(12):3721.
[40] Chu B, Harney PJ, Li Y, Linliu K, Yeh F, Hsiao BS. Rev Sci Instrum 1994;65(3):597.

[41] Hsiao BS, Chu B, Yeh F. NSLS Newslett 1997;July:1.
[42] Wilchinsky ZM. J Appl Phys 1960;31(11):1969.
[43] Abramowitz M, Stegun Irene A. Handbook of Mathematical Functions with Formulas, Graphs and Mathematical Tables US Department of Commerce, National Bureau of Standards. Applied Mathematics Series: 55, 1964. 1045 pp.
[44] Radler MJ, Landes BG, Nolan SJ, Broomall CF, Chritz TC, Rudolf PR, Mills ME, Bubeck RA. J Polym Sci: Part B: Polym Phys 1994;32:2567.
[45] Dean DM, Rebenfeld L, Register RA, Hsiao BS. J Mater Sci 1998;33:1.
[46] Provost RL. US Patent 4,144,023, 1977.
[47] Konopasek L, Hearle JWS. J Appl Polym Sci 1977;21:2791.
[48] Morgan RJ, Pruenda CO, Steele WJ. J Polym Sci, Polym Phys Ed 1983;21:1757.
[49] Grubb DT, Prasad K, Adams W. Polymer 1991;32(7):1167.
[50] Ruland W. J Polym Sci Part C 1969;28:143.